$2p_{3/2}^{-1}3x^{-1}$–$3x^{-1}3d^{-1}$ X-ray satellites spectra in the Lα_1 region of 4d transition elements

Surendra Poonia*[a] and S N Soni[b]

[a]Division of Natural Resources and Environment, Central Arid Zone Research Institute, Jodhpur-342 003, Rajasthan, India
[b]X-ray Laboratory, Physics Department, Jai Narain Vyas University, Jodhpur-342 005, Rajasthan, India

E-mail : poonia.surendra@gmail.com

Abstract : The X-ray satellite spectra arising due to $2p_{3/2}^{-1}3x^{-1}$–$3x^{-1}3d^{-1}$ ($x \equiv s$, p, d) transition array, in elements with Z = 40 to 48, have been calculated, using available Hartree-Fock-Slater (HFS) data on $1s^{-1}$–$2p^{-1}$ $3x^-$ and $2p_{3/2}^{-1}$–$3x^{-1}$,$3x^{-1}$ Auger transition energies. The relative intensities of all the possible transitions have been estimated by considering cross – sections for the Auger transitions simultaneous to a hole creation and then distributing statistically the total cross sections for initial two hole states $2p_{3/2}^{-1}$–$3x^{-1}$ amongst various allowed transitions from these initial states to $3x^{-1}$ $3d^{-1}$ final states by Coster-Kronig (CK) and shake off processes. In both these processes initial single hole creation is the prime phenomenon. Each transition has been assumed to give rise to a Gaussian line and the overall spectrum has been computed as the sum of these Gaussian curves. The calculated spectra have been compared with the measured satellite energies in Lα_1 spectra. Their intense peaks have been identified as the observed satellite lines. The peaks in the theoretical satellite spectra were identified as the experimentally reported satellites α_3, α_4 and α_5, which lie on the high-energy side of the Lα_1 dipole line.

Keywords : Lα_1 X-ray satellites, M vacancy Lα transitions, X-Ray emission spectra

PACS Nos. : 32.20Rj and 78.70E

1. Introduction

For several past years, the identification of the transitions in doubly and triply inner shell ionized atoms, which can be assigned to various X-ray satellites [1-7], has been in progress in this laboratory. The method adopted is more reliable than Wentzel's Z+1 approximation [8,9]. The transition energies have been calculated using Hartree-Fock-Slater (HFS) model

---

* Corresponding Author

[10] in the intermediate coupling scheme and their relative intensities have been estimated in the L-S coupling scheme. In continuation of the same work, we present here the transition assignments to the satellites named α_3, α_4 and α_5 in the L-emission spectra of 4d transition elements.

A survey of the literature reveals that six decades ago Parratt [11] reported the high-resolution measurement for the complete L X-ray spectrum of Silver. This work has been extended by McGuire [12], who used radiative, Coster-Kronig and Auger transition rates and Wentzel's hypothesis to compute the Ag L X-ray satellite spectrum. The same spectrum has been interpreted on the basis of one addition of M and N shell vacancy by Chen *et al.* [13]. In the spectrum of silver, four lines reported on high energy side of and comparatively far away from Lα line have been identified by Soni [14] as hypersatellites. Krause *et al.* [15] have interpreted the L X-ray emission spectrum of $_{40}$Zr in terms of an extra M_3 or M_5 vacancy.

The study of Lα X-ray satellites, in particular, has been performed by Kallne [16], reported a complex satellite structure appearing on the high energy side of Nb L$\alpha_{1,2}$ emission lines, and it is interpreted as due to $L_3M - MM_{4,5}$ double-vacancy transitions. On the other hand, Juslen *et al.* [17] has presented the pure satellite structure on the high-energy side of the diagram line L$\alpha_{1,2}$ of the elements $_{40}$Zr to $_{48}$Cd. The same satellite structure has been interpreted on the basis of L_1–$L_3M_{4,5}$ Coster Kronig transitions and shake-off by Putila *et al.* [18] in the elements $_{49}$In and $_{50}$Sn. Tulkki *et al.* [19] have recently reported the calculated Lα satellite spectra for the elements $_{40}$Zr, $_{45}$Rh and $_{47}$Ag. They conclude that the theoretically constructed spectra compared with experimental results are in good overall agreement with respect to both the energy and intensity distribution, but there are discrepancies between the experimental and theoretical shapes. Very recently the L – emission spectrum of $_{74}$W has attracted the attention of two Laboratories in the world and highly sophisticated analysis of the satellites in Lα spectra. The L spectrum of tungsten was studied by Vlaicu *et al.* [20], who have made few addressing contributions to the L$\alpha_{1,2}$ line shapes from satellites due to N – shell spectator hole transitions. The study of Diamant *et al.* [21] has presented the Lα' satellite of tungsten due to M_5 spectator hole transitions and have also presented [22] the L$\alpha_{1,2}$ line shapes can be well accounted for by the fully split diagram transition $2p_{3/2}{}^{-1} \rightarrow 3d_{3/2,5/2}{}^{-1}$ alone, without involving contributions from any spectator hole transition. The recent study of Czarnota *et al.* [23] has presented the observed M-shell satellite structure of L$\alpha_{1,2}$ X-ray transitions of $_{42}$Mo and $_{46}$Pd induced by an impact of O and Ne ions by one- and two- vacancy configurations for oxygen ions. The similar study of Czarnota *et al* [24] has also presented the measured X-ray satellite structure of Pd L$\alpha_{1,2}$ ($L_3M_{4,5}$) transitions excited by an impact of O^{7+} and Ne^{6+} iosn with energy 279 and 178 MeV, respectively.

In this paper, we report the results of our calculations on the high-energy X-ray satellites in Lα_1 spectra of 4d transition elements. The complete data have been compiled by Cauchois and Sénémaud [25]. These data have been graphically presented in Figure 1, in which the energies of satellites relative to the respective α_1 lines have been plotted against Z.
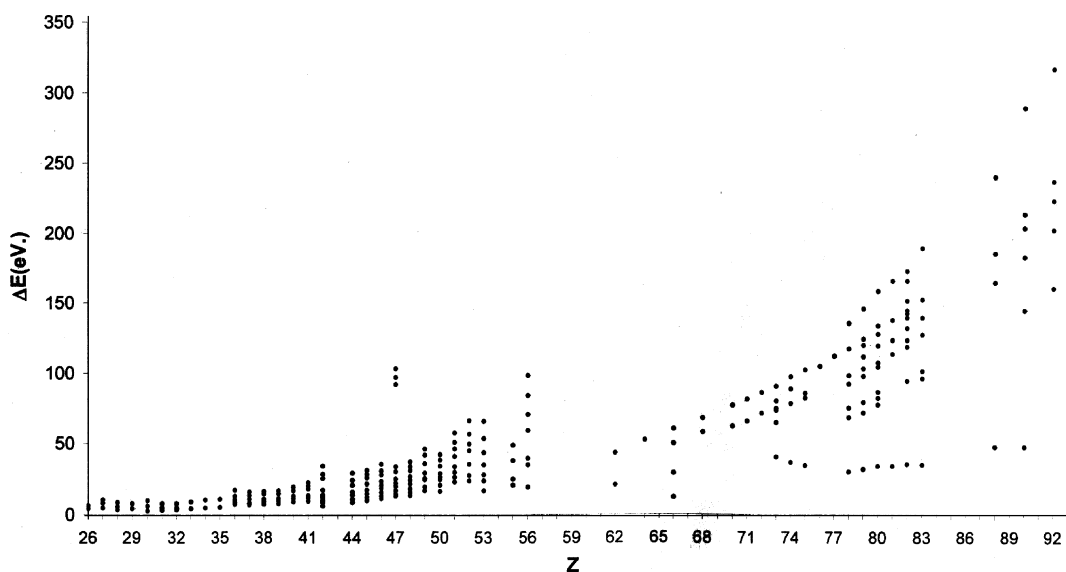
Figure 1. Measured energies of various satellites on high energy side of Lα_1 line relative to their respective α_1 energies.

2. Calculation

We have undertaken studies of all those transitions of $2p_{3/2}^{-1}3x^{-1}$–$3x^{-1}3d^{-1}$ ($x \equiv s, p, d$) array which are allowed according to selection rules [10] $\Delta L = 0, \pm 1$, $\Delta S = 0$ and $\Delta J = 0, \pm 1$. We have calculated their Hartree-Fock-Slater (HFS) energies in intermediate coupling and their relative probabilities in L-S coupling scheme. Parente *et al.* [26] and very recently Diamant *et al.* [21] and Oohashi *et al.* [27] proved that relative probabilities in L-S coupling is more suitable in 3d and 4d transition elements while *j–j* coupling should be applied to elements at the end of the periodic Table. We have computed the spectra arising out of the superposition of these transitions in the spectra of an element by assuming each transition to give rise to a Gaussian line. Finally, these computed spectra have been compared with the observed satellite spectra [25].

(2.1) The transition energies :

The energies of the transitions, used in the present study, have been calculated by the combination formula :

$$E\left(2p_{3/2}^{-1}3x^{-1} - 3x^{-1}3d^{-1}\right) = E(K\alpha_1) - E\left(1s^{-1} - 2p_{3/2}^{-1}3x^{-1}\right) + E\left(2p_{3/2}^{-1} - 3x^{-1}3d^{-1}\right) \quad (1)$$

where $E(K\alpha_1)$ is the energy of $K\alpha_1$ line. Its values have been taken from the Tables of Bearden and Burr [28]. $E\left(1s^{-1} - 2p_{3/2}^{-1}3x^{-1}\right)$ and   are the Auger electron energies for the   and $2p_{3/2}^{-1} - 3x^{-2}$ transitions respectively. These energies have been taken from the Table of Larkins [29], who has calculated various two-hole state

energies of atoms with Z = 10–100 in the intermediate coupling approximation and has, also, corrected them for adiabatic relaxation [30] of the orbitals due to a sudden creation of an inner hole as well as for the solid-state effect [31] of the sample. His values are in good agreement with the available experimental Auger electron energy data in the region of Z values, presently under study, as claimed by Larkins [29].

2.2. The transition probabilities :

For the emission of Lα satellites, in hand, those transitions are being considered in which the initial states are doubly ionized, one vacancy lying in $2p_{3/2}$ sub-shell and second one in any of M-sub-shells. Such states are formed by two processes.

(i) $2s^{-1}$–$2p_{3/2}^{-1}3x^{-1}$ Coster-Kronig transitions, namely conversion of one-hole state $2s^{-1}$ to a two hole state $2p_{3/2}^{-1}3x^{-1}$ ($x \equiv s, p, d$) through the Auger transition $2s^{-1}$–$2p_{3/2}^{-1}3x^{-1}$.

(ii) By shake-off process, namely an electron from M-shell of the atom may escape out simultaneous to the formation of a $2p_{3/2}$ vacancy. This additional vacancy is created due to shaking of the atomic orbits caused by a sudden change in the potential field in the atom, taking place when a $2p_{3/2}$ electron leaves the atom with a fast speed.

In both these processes the initial single hole creation is the prime phenomenon. Various efforts have been made for calculating, theoretically, the cross sections for such single ionization. Moores *et al.* [32] have presented formulas for these cross-sections in which electron bombardment has been the primary source of energy. Their formula for probability of formation of a hole in a 'nl' state, is

$$\sigma_{nl} = \left(\pi \, n^4 a_0^2 \, Z_{nl} / Z^4 \right) \sigma_{nl}(R) \tag{2}$$

or, say

$$\sigma_{nl} = \left(1.628 * 10^{-14} \right) Z_{nl} \, \sigma_{nl}(R) / E_{nl}^2 \tag{3}$$

In these formulas *n* and 1 denote the sub-shell of the atom in which a hole is created, Z_{nl} denotes the total number of electrons in this sub-shell and E_{nl} denotes the binding energy of the electron in this sub-shell.   is known as reduced cross-section, and is calculated by the formula given in eq. (4)

$$\sigma_{nl}(R) = (1/u) \left[A \ln u + B(1 - 1/u)^2 + \left(C/u + D/u^2 \right)(1 - 1/u) \right]. \tag{4}$$

The A, B, C and D are constants, whose values for ionization in $2s_{1/2}$ sub-shell are $A = 0.823$, $B = 3.69$, $C = 0.62$, $D = 1.79$ and in $2p_{3/2}$ sub-shell are $A = 0.530$, $B = 5.07$, $C = 1.20$ and $D = 2.50$ [Ref. 32]. The dimensionless parameter *u* denotes the ratio : $u = E_0 / E_{ml}$ = Incident energy of incoming electron /Binding Energy of the *nl* electron.

We have calculated the values of   for initial single hole states, namely $2s_{1/2}{}^{-1}$ and $2p_{3/2}{}^{-1}$, involved in the present study by using these formulas.

Since different researchers, who have measured satellite spectra of various elements experimentally, have used different excitation energies, we have taken arbitrarily the value of *u* as 2.5, a practical value found [33] to give a measurable intensity of satellites.

We understand that after creation of a single hole state, it is the probability of a particular subsequent process that will lead to the formation of two-hole state. If the single hole so created gets converted through a Coster Kronig transition, to a double hole state, the probability of formation of double hole state via this process is written as $\sigma.\sigma'$, where   is the $2s_{1/2}$ sub-shell ionization cross section of the atom and   is the probability of its decay through the CK transition $2s^{-1}-2p_{3/2}{}^{-1}3x^{-1}$.

The value of   , so calculated, has been multiplied with Coster-Kronig transition probability   , taken from table of McGuire [34]. It should be noted that the Coster-Kronig transitions help in forming only $2p_{3/2}{}^{-1}-3d^{-1}$ states, and that too only in the elements[32] up to $Z=47$. The other $2p_{3/2}{}^{-1}-3x^{-1}$ transitions are not allowed energetically in these elements. Further, no such Coster Kronig transitions take place in elements [34] with $Z=48$ to 73.

Coming to shake-off process, we have first calculated the cross – section using formulas given in Eqs. (2) to (4) and have, then, multiplied it with the shake-off probability of a M-sub-shell electron. This probability has been calculated by interpolation from the percentage probabilities of shake-off processes occurring with a single photo-ionization in inert gases [35].

$\sigma(2p_{3/2}{}^{-1})$

Subsequently the total probability of creation of an initial state $2p_{3/2}{}^{-1}\,3x^{-1}$ has been determined by adding these two cross – sections as, calculated above.

The cross – section for a set of $2p_{3/2}{}^{-1}\,3x^{-1}$ levels with *x* denoting any one sub-shell of *M* - shell, so calculated, has been assumed as the total probability of all the transitions from this set. This has been distributed statistically among all the allowed transitions from this set of levels, considering first all the multiplets of super-multiplets from various $^{(2S+1)}$(L) levels of the set and then using tables of White and Eliason for relative probabilities of the transitions of each multiplet, as given by Condon and Shortley [Ref. 10] for relative probabilities of the transitions of each multiplet. The detailed method of this distribution have been used by Poonia and Soni in our earlier reports [1-7].

2.3. Synthesis of the spectrum :

We have calculated energies and intensities of all the possible transitions of the $2p_{3/2}{}^{-1}3x^{-1}-3x^{-1}\,3d^{-1}$ ($x \equiv s,\ p,\ d$) array as mentioned above. The transitions having intensity less than 1/10th of the maximum intensity out of all of them have been ignored. A composite spectrum formed by spectral lines emitted by these transitions has been computed by taking each as a Gaussian line. The choice of a Gaussian shape has been

favoured over the Lorentzian one as it is more suitable to satellite spectra, as discussed by Maskil and Deutsch [36]. For this, we have taken energy on X-axis and intensity on Y-axis. The peak height of each line is taken equal to the relative intensities and the peak position on X-axis is taken at the energy of the transition. The widths of all the lines in one element have been assumed equal and its value has been decided by trial and error method in such a way that the number of peaks obtained from the calculated spectrum is at least equal to or greater than the number of satellites observed experimentally in the spectrum of the element. The computed spectra in this case of two representative elements, $_{40}$Zr and $_{48}$Cd, thus obtained, are shown in Figures 2-3. In these spectra peaks of higher intensities have been recognized as the observed satellites. For the one to one correspondence between peaks and measured satellites, the relative energy separations of peaks and those of measured satellites have been taken into consideration.
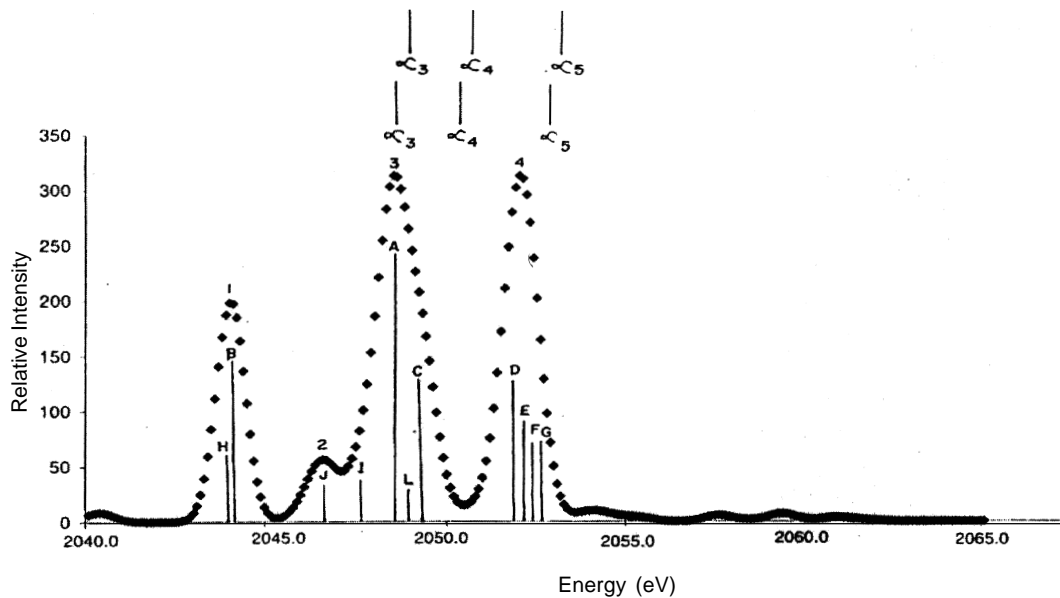
Figure 2. Calculated $2p_{3/2}^{-1}3x^{-1}$–$3x^{-1}3d^{-1}$ ($x \equiv s$, p, d) spectrum of $_{40}$Zr. The measured $L\alpha_1$ satellites are shown in two rows at the top. The upper rows of bars are marked at energies taken from [Ref. 25]. In the lower row, these are marked after shifting the zero so that agreement between measured satellites and calculated peaks becomes obvious.

3.   Results and disucssion

Out of all the 49 transitions of $2p_{3/2}^{-1}3x^{-1}$–$3x^{-1}3d^{-1}$ ($x \equiv s$, p, d) array, 12 belonging to $x = d$ group have such intensities so as to warrant attention. These are presented in Table 1. in order of decreasing intensity and are named A through L. The main transitions responsible for the formation of such peaks with their relative intensities, their calculated energies, heights and energy positions of computed peaks and measured satellite energies are presented in Tables 2-4. All these transitions in the element $_{40}$Zr have energies and intensities such that a superposition of corresponding Gaussian lines gives rise to a

Table 1. Relative intensities of the transitions of $2p_{3/2}^{-1}3x^{-1}$–$3x^{-1}3d^{-1}$ ($x \equiv s$, p, d) array for Z = 40–48. The names are denoted in the text. In $_{40}$Zr, both the Coster-Kronig transitions and Shake-off probabilities are added, while in $_{48}$Cd, Coster Kronig transitions are not allowed energetically.

S. No.	Transition (a)	Symbol of the transition used in the text	Relative Intensity Z = 40 (b)	Relative Intensity Z = 41 (b)	Relative Intensity Z = 42 (b)	Relative Intensity Z = 44 (b)	Relative Intensity Z = 45 (b)	Relative Intensity Z = 46 (b)	Relative Intensity Z = 47 (b)	Relative Intensity Z = 48 (b)
1	$^3F_4$–$^3F_4$ (3d)	A	242.9	197.5	152.1	120.1	108.7	97.3	88.3	12.3
2	$^1D_2$–$^1D_2$ (3d)	B	143.9	117.0	90.1	71.2	64.4	57.6	52.3	7.3
3	$^1F_3$–$^1G_4$ (3d)	C	129.5	105.3	81.1	64.0	58.0	51.9	47.1	6.5
4	$^3D_3$–$^3F_4$ (3d)	D	129.4	105.2	81.0	64.0	57.9	51.8	47.0	6.5
5	$^3D_2$–$^3F_3$ (3d)	E	89.4	72.7	55.9	44.2	40.0	35.8	32.5	4.5
6	$^1P_1$–$^1D_2$ (3d)	F	71.9	58.5	45.0	35.6	32.2	28.8	26.2	3.6
7	$^1F_3$–$^1D_2$ (3d)	G	71.9	58.5	45.0	35.6	32.2	28.8	26.2	3.6
8	$^3D_3$–$^3P_2$ (3d)	H	60.4	49.1	37.8	29.9	27.0	24.2	22.0	3.0
9	$^3P_1$–$^3P_2$ (3d)	I	35.9	29.2	22.5	17.8	16.1	14.4	13.1	1.8
10	$^3D_2$–$^3P_1$ (3d)	J	32.4	26.4	20.3	16.0	14.5	12.9	11.8	1.6
11	$^3P_1$–$^3P_0$ (3d)	K	28.8	23.4	18.0	14.2	12.9	11.5	10.5	1.4
12	$^3P_0$–$^3P_1$ (3d)	L	28.8	23.4	18.0	14.2	12.9	11.5	10.5	1.4

a. The spectator hole position has been shown in the braces along with the transitions.
b. The relative intensities of Coster Kronig transitions and shake off probabilities.
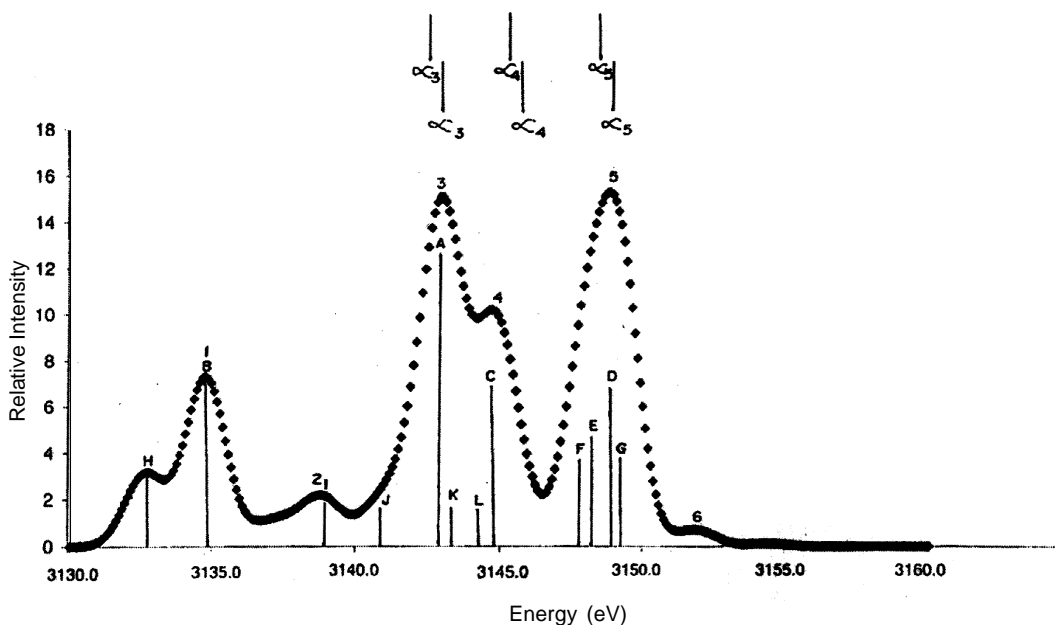
Figure 3. Computed $2p_{3/2}^{-1}3x^{-1}$–$3x^{-1}3d^{-1}$ ($x \equiv s$, p, d) spectrum of $_{48}$Cd. For bars at the top, see captions to Figure 2..

Table 2. The calculated energy and height of peak no. 3, and of the transitions A and K which gives rise to this peak. The corresponding values of measured α_3 energy are also shown.

S No.	Z	A ($^3F_4 - ^3F_4$)		K ($^3P_1 - ^3P_0$)		Computed peak data Peak no. 3		Measured α_3 energies (eV)
		Relative Intensity	Energy (eV)	Relative Intensity	Energy (eV)	Relative Intensity	Energy (eV)	
1	40	243.96	2048.5	28.82	2048.1	311.15	2048.6	2048.9
2	41	197.50	2172.4	23.40	2172.6	253.85	2172.3	2172.4
3	42	152.12	2300.0	18.04	2299.9	194.52	2300.1	2298.3
4	44	120.15	2566.1	14.25	2566.2	153.3	2566.3	2565.4
5	45	108.70	2704.8	12.90	2705.0	125.58	2704.9	2704.1
6	46	97.31	2846.9	11.54	2847.8	112.83	2847.0	2846.2
7	47	88.34	2993.2	10.47	2993.5	102.95	2993.3	2992.4
8	48	12.28	3142.9	1.45	3143.3	14.87	3143.1	3142.5

spectrum consisting of 4 peaks, the number is increasing with a rise in Z by reaching to 6 in $_{48}$Cd. The computed satellites spectra in this case of two representative elements, $_{40}$Zr and $_{48}$Cd, are shown in Figures 2-3. The three most intense peaks in these computed spectra have been marked as no. 3, 4 and 5. A comparison of the computed spectrum of an element with the measured satellite spectrum reveals that whereas the measured satellite energies are close to those of intense peaks, their separations in the computed
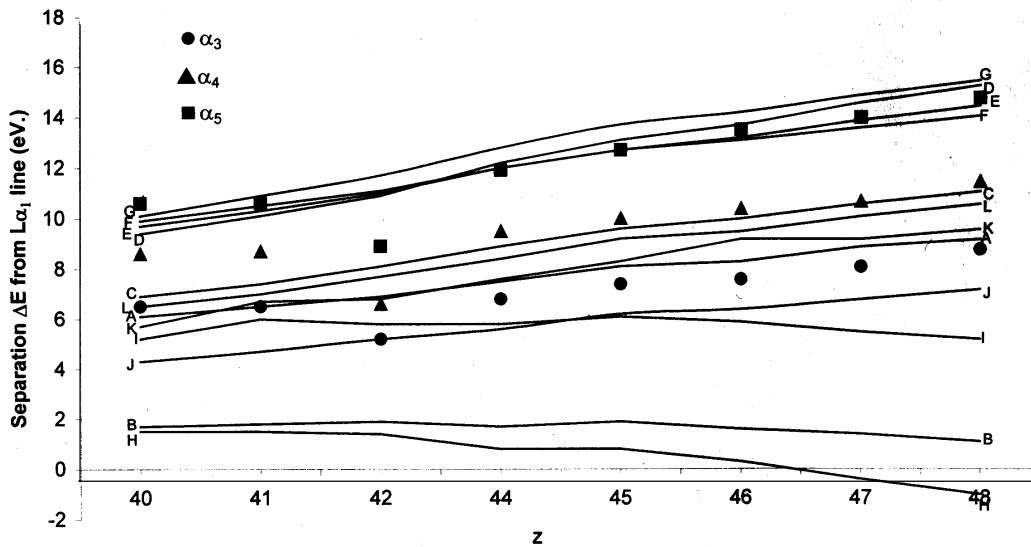
Figure 4. Variation of calculated transition energies with Z. The measured spectra of elements with Z = 40–48 are also shown, after shifting their zeros, as in Figures 2-3, such that these agree with the interpolated values of peak energies of calculated spectra.

Table 3. The calculated energy and height of peak no. 3 and 4, and of the transitions C and L, which forms these peak. The satellite α_3 and α_4 to which this peak is identified are also shown.

S No.	Z	C ($^1F_3$–$^1G_4$)		L ($^3P_0$–$^3P_1$)		Computed peak data Peak no. 3 and 4		Measured α_3 and α_4 energies (eV)
		Relative Intensity	Energy (eV)	Relative Intensity	Energy (eV)	Relative Intensity	Energy (eV)	
1	40	129.52	2049.3	28.82	2048.9	311.50	2048.6	2048.9 (α_3)
2	41	105.3	2173.3	23.4	2172.9	253.85	2172.3	2172.4 (α_3)
3	42	81.10	2301.2	18.04	2300.8	112.41	2301.2	2299.7 (α_4)
4	44	64.06	2567.5	14.25	2567.0	94.95	2567.4	2568.1 (α_4)
5	45	58.0	2706.3	12.90	2705.9	81.19	2706.2	2706.7 (α_4)
6	46	51.87	2848.6	11.54	2848.1	74.99	2848.4	2849.0 (α_4)
7	47	47.10	2994.9	10.47	2994.4	70.04	2994.7	2995.0 (α_4)
8	48	6.54	3144.8	1.45	3144.3	9.95	3144.9	3145.2 (α_4)

and measured spectra are in good mutual agreement. The computed $L\alpha_1$ satellites spectra are also presented in Figures 2-3, in each of which the measured satellite data are shown in terms of vertical bars in two rows at the top of the figure. In the upper row the measured[24] satellite position is shown while in the lower row the measured data have been shown after shifting them horizontally by the average of the discrepancies in measured and computed peak energies. This agreement in all the elements, studied presently, is also shown in Figure 4. wherein is also presented the positions of measured satellites α_3, α_4 and α_5 in these spectra. These figures also give a clear view of one to one correspondence between the measured satellites and intense transitions of calculated spectra. The transition assignments made to the satellites based on the identification of the peaks are discussed below.

3.1. $2p_{1/2}^{-1}3d^{-1} - 3d^{-2}$ array :

3.1.1. Transitions A and K :

Out of these two transitions, the transition A namely $^3F_4$–$^3F_4$, is the most intense among the 12 transitions listed in Table 1, of the complete $2p_{3/2}^{-1}3x^{-1}-3x^{-1}3d^{-1}$ array. This transition gives rise to the highest peak in each of the spectra, marked no. 3 (Figures 2-3). This is identified as the satellite α_3 in the spectra of $_{40}$Zr to $_{48}$Cd. The transition K ($^3P_1$–$^3P_0$) is the weakest transition of the twelve transitions A–L of the $2p_{3/2}^{-1}3x^{-1}-3x^{-1}3d^{-1}$ array, and it has the energy close to those of A in the range of Z = 40 to 48. It also contributes in forming the peak no. 3 in all the spectra and hence will be taken as the supporting origin for the line α_3.

Table 4. The calculated energy and height of transitions D, E, F and G and of corresponding peak no. 4 and 5. The satellite α_5 with which this peak is identified are also shown.

S No.	Z	D ($^3D_3$–$^3F_4$)		E ($^3D_2$–$^3F_3$)		F ($^1P_1$–$^1D_2$)		G ($^1F_3$–$^1D_2$)		Computed peak data Peak no. 4 and 5			Measured α_5 energies (eV)
		Energy (eV)	Relative Intensity	Energy (eV)	Relative Intensity	Energy (eV)	Relative Intensity	Energy (eV)	Relative Intensity	Peak	Energy (eV)	Relative Intensity	
1	40	2051.8	129.38	2052.1	89.40	2052.3	71.96	2052.5	71.96	4	2052.1	309.74	2053.0
2	41	2176.0	105.20	2176.2	72.70	2176.4	58.50	2176.8	58.50	4	2176.2	253.30	2176.5
3	42	2304.0	81.00	2304.1	55.97	2304.2	45.05	2304.8	45.05	5	2304.2	201.53	2302.0
4	44	2570.8	63.98	2570.6	44.21	2570.6	35.58	2571.4	35.58	5	2570.9	164.40	2570.5
5	45	2709.8	57.90	2709.4	40.0	2709.4	32.20	2710.4	32.2	5	2709.8	145.60	2709.4
6	46	2852.3	51.81	2851.8	35.80	2851.7	28.82	2852.8	28.82	5	2852.2	122.75	2852.1
7	47	2998.9	47.04	2998.2	32.50	2997.9	26.16	2999.2	29.16	5	2998.8	110.62	2998.3
8	48	3149.0	6.54	3148.2	4.51	3147.8	3.63	3149.2	3.63	5	3148.9	15.19	3148.5

3.1.2. Transitions C and L :

In the elements Z = 40 to 48 the transitions C ($^1F_3$–$^1G_4$) and L ($^3P_0$–$^3P_1$) of the $2p_{3/2}^{-1}$ $3d^{-1}$–$3d^{-2}$ array and some weaker ones contribute to peak no. 3 in $_{40}$Zr and no. 4 in $_{42}$Mo to $_{48}$Cd (Figures 2-3), in the order of energy increase. The transition C is closer to A in $_{40}$Zr, and gradually shifts towards the peak no. 4 as Z increases. It, therefore, adds to peak no. 3 in $_{40}$Zr, forms a shoulder in $_{42}$Mo and $_{44}$Ru and, transition C gives rise to a well-separated peak, marked as no. 4 in $_{46}$Pd to $_{48}$Cd. In the spectrum of $_{40}$Zr, the measured position of α_4 is between these peaks. While, in those of $_{42}$Mo to $_{48}$Cd, peak no. 4 is identified as α_4. The transition L, namely $2p_{3/2}^{-1}3d^{-1}$ $^3P_0$–$3d^{-2}$ $^3P_1$ has energy close to it on its lower side. Hence it can be taken as a supporting origin for the line α_4.

3.1.3. Transition D, E, F and G :

The set of transitions $^3D_3$–$^3F_4$, $^3D_2$–$^3F_3$, $^1P_1$–$^1D_2$ and $^1F_3$–$^1D_2$, named D, E, F and G respectively have energies so close to one another that in the spectra, under present study, these gives rise to a combined peak, marked no. 4 in the spectra of $_{40}$Zr (Fig. 2) and no. 5 in other spectra $_{42}$Mo to $_{48}$Cd (Fig. 3). This peak has intensity nearly equal to the highest intensity peak, no. 3, discussed above (§ 3.1.2). This peak is, hereby, identified as the satellite in the spectra of $_{40}$Zr to $_{48}$Cd.

3.1.4. Transition B and H :

The second most intense transition B and another intense transition H in the array $2p_{3/2}^{-1}3d^{-1}$–$3d^{-2}$ considered presently is $^1D_2$–$^1D_2$ and $^3D_3$–$^3P_2$, in Table 3. It gives rise to a well-separated peak, marked no. 1, in each of the calculated spectra presented in Figures 2-3. This peak merges with $L\alpha_{1,2}$ line in all these spectra and, hence, is not observed independently.

3.1.5. Transitions I and J :

The transitions shown at sr. no. 9 and 10 in Table 3 have energies lying in the range of the above-mentioned transitions, A-L, though its intensity is low, it gives rise to a well-separated peak, marked no. 2 due to its energy, in each of the spectra presented in Figures 2-3. However, no line has been observed corresponding to this peak.

4. Conclusion

The present studies have revealed that all three satellites α_3, α_4 and α_5 observed in $L\alpha_1$ spectra of 4d transition elements, with a few exceptions, arise mainly due to $2p_{3/2}^{-1}$–$3d^{-1}$ transitions in the presence of a 3d spectator vacancy. The association of various intense transitions of the array with the measured satellites is presented in Table 5. On the basis of agreement between the computed spectra and measured satellites, it is observed that the satellite α_3 is observed due to intense transition, $^3F_4$–$^3F_4$, in order of decreasing contribution of intensity. It has been found that the transition $^1F_3$–$^1G_4$ is the main source of the emission of the satellite α_4 in the elements $_{42}$Mo to $_{48}$Cd. The line

Table 5. The Lα satellites and corresponding $2p_{3/2}^{-1}3x^{-1}$–$3x^{-1}3d^{-1}$ ($x \equiv s$, p, d) transitions in elements $_{40}$Zr to $_{48}$Cd.

S No.	Z Satellites	Transitions							
		40	41	42	44	45	46	47	48
1	α_3	A,C,K,L	A,C,K,L	A,K	A,K	A,K	A,K	A,K	A,K
2	α_4	–	–	C,L	C,L	C,L	C,L	C,L	C,L
3	α_5	D,E,F,G	D,E,F,G	D,E,F,G	D,E,F,G	D,E,F,G	D,E,F,G	D,E,F,G	D,E,F,G

α_5, observed in the spectra of elements with Z = 40–48, has been assigned to the $^3D_3$–$^3F_4$, $^3D_2$–$^3F_3$, $^1P_1$–$^1D_2$ and $^1F_3$–$^1D_2$ transitions. Unfortunately no experimental data are available on the intensities, of these satellites.

References

[1] S N Soni *X-ray Spectroscopy and Allied Areas,* S K Joshi, B D Shrivastava and A P Deshpande (Eds.), (New Delhi : Narosa Pub. House) p. 5 (1998). This is a review report and contains a list of the papers published by the author on this subject in the period (1980-1997)

[2] S Poonia and S N Soni *Indian J. Pure Appl. Phys.* **38** 133 (2000)

[3] S N Soni and S Poonia *J. Phys. Chem. Solids* **61** 1509 (2000)

[4] S Poonia and S N Soni *J. Phys. Chem. Solids* **62** 503 (2001)

[5] S Poonia and S N Soni *J. Electron Spectrosc. Relat. Phenom.* **122** 27 (2002)

[6] S N Soni and S Poonia *Indian J. Phys.* **76B** 11 (2002)

[7] S Poonia and S N Soni *Indian J. Pure Appl. Phys.* **40** 786 (2002)

[8] G Wentzel *Ann. Phys. Ny* **66** 437 (1921)

[9] G Wentzel *Zeits Physik* **31** 445 (1925)

[10] E U Condon and G H Shortley *The Theory of Atomic Spectra* (Cambridge : Cambridge University Press) p. 241 (1967)

[11] L G Parratt *Phys. Rev.* **54** 99 (1938)

[12] E J McGuire *Phys. Rev.* **A5** 2313 (1972)

[13] M H Chen, B Crasemann, M Aoyagi and H Mark *Phys. Rev.* **A15** 2312 (1977)

[14] A N Nigam and S N Soni *Nat. Acad. Sci. Letters* **2(4)** 145 (1979)

[15] M O Krause, F Wuilleumier and C W Nestor *Phys. Rev.* **A6** 871 (1972)

[16] E Kallne and M Pessa *J. Phys. C : Solid State Phys.* **8** 1985 (1975)

[17] H Juslen, M Pessa and G Graeffe *Phys. Rev.* **A 19(1)** 196 (1979)

[18] P Putila, H Juslen, M Pessa and G Graeffe *Physica Scripta* **20** 41 (1979)

[19] J Tulkki and O Keski-Rahkonen *Phys. Rev.* **A24** 849 (1981)

[20] A M Vlaicu, T Tochio, T Ishizuka, D Ohsawa, Y Ito, T Mukoyama, A Nisawa, T Shoji and S Yoshikado *Phys. Rev.* **A58(5)** 3544 (1998)

[21] R Diamant, S Huotari, K Hamalainen, R Sharon, C C Kao and M Deutsch *J. Phys. B: Atom. Mol. Opt. Phys.* **33** L649 (2000)

[22] R Diamant, S Huotari, K Hamalainen, R Sharon, C C Kao and M Deutsch *Phys. Rev.* **A63(2)** 022508 (2001)

[23]   M Czarnota, M Pajek, D Banas, D Chmielewska, J Rzadkiewicz, Z Sujkowski, J-C1 Dousse, M Berset, O Mauron, Y–P Maillard, P A Raboud, J Hoszowska, M Polasik, and K Slabkowska *Nucl. Inst. Meth. Phys. Res.* **B205** 133 (2003)

[24]   M Czarnota, M Pajek, D Banas, J-C1 Dousse, Y–P Maillard, O Mauron, P A Raboud, M Berset, D Chmielewska, J Rzadkiewicz, Z Sujkowski, J Hoszowska, K S Slabkowska and M Polasik *Braz. J. Phys.* **36(2B)** 546 (2006)

[25]   Y Cauchois and C Sénémaud *Wavelengths of X-ray Emission Lines and Absorption Edges* (2nd Edition) p. 217 (Oxford : Pergamon Press) (1978)

[26]   F Parente, Mau Hsiung Chen, B Crasemann and H Mark *At. Data Nucl. Data Tables* B383 (1981)

[27]   H Oohashi, Y Ito, T Tochio, A M Vlaicu, H Yoshikawa and S Fukushima *Rad. Phys. and Chem.* **75(11)** 1510 (2006)

[28]   J A Bearden and A F Burr *Rev. Mod. Phys.,* **39** 78 (1967)

[29]   F P Larkins *At. Data Nucl. Data Tables* **20** 311 (1977)

[30]   D A Shirley *Phys. Rev.* **A7** 1520 (1973)

[31]   F P Larkins *J. Phys. C (GB)* **10** 2453 (1977)

[32]   D L Moores, L B Golden and D H Sampson *J. Phys.* **B13** 385 (1980)

[33]   S N Soni, Ph.D. Thesis, (Jai Narain Vyas University, Jodhpur), India (1979)

[34]   E J McGuire, L-sheel Auger, Coster Kronig and Radiative Matrix elements, Report No. SC-RR-710075, Sandia Laboratories (1971)

[35]   T A Carlson and C W Nestor *Jr. Phys. Rev.* **A8** 2887 (1972)

[36]   N Maskil and M Deutsch *Phys. Rev.* **A38** 3467 (1988)